



## Article

# All-Fiber High-Energy Mode-Locked Ytterbium-Doped Fiber Laser with Bismuth Telluride Nanosheet Saturable Absorber

Hazlihan Haris <sup>1,\*</sup>, Malathy Batumalay <sup>2</sup>, Tan Sin Jin <sup>3</sup>, Ahmad Razif Muhammad <sup>4</sup> , Arni Munira Markom <sup>5</sup>,  
Muhamad Hakim Izani <sup>4</sup>, Megat Muhammad Ikhsan Megat Hasnan <sup>1</sup>  and Ismail Saad <sup>1,\*</sup>

<sup>1</sup> Faculty of Engineering, Universiti Malaysia Sabah (UMS), Kota Kinabalu 88400, Sabah, Malaysia

<sup>2</sup> Faculty of Data Science & IT, INTI International University, Nilai 71800, Negeri Sembilan, Malaysia

<sup>3</sup> School of Engineering, UOW Malaysia KDU University College, Shah Alam 40150, Selangor, Malaysia

<sup>4</sup> Institute of Microengineering and Nanoelectronics (IMEN), Universiti Kebangsaan Malaysia (UKM),  
Bangi 43600, Selangor, Malaysia

<sup>5</sup> School of Electrical Engineering, College of Engineering, Universiti Teknologi MARA, Cawangan Johor,  
Kampus Pasir Gudang, Masai 81750, Johor, Malaysia

\* Correspondence: hazlihanharis@ums.edu.my (H.H); ismail\_s@ums.edu.my (I.S)

**Abstract:** Utilizing bismuth telluride ( $\text{Bi}_2\text{Te}_3$ ) nanosheet saturable absorbers (SA), a remarkable source of continuous-wave infrared radiation known for its high efficiency and wide range of accessible wavelengths, has been successfully developed. The mode-locking bright pulses have a repetition frequency of 9.5 MHz and a pulse width of 0.6 ps at a power level of 203.5 mW. The optical spectrum has its center at 1050.23 nm and delivers pulse energies of 2.13 nJ and output power of 20.3 mW. Using a straightforward 18 m long ring design and a laser cavity with a  $-19.9 \text{ ps}^2/\text{km}$  dispersion, a 44 dB signal-to-noise ratio (SNR) was achieved to demonstrate the pulse's strong stability.



**Citation:** Haris, H.; Batumalay, M.; Jin, T.S.; Muhammad, A.R.; Markom, A.M.; Izani, M.H.; Hasnan, M.M.I.M.; Saad, I. All-Fiber High-Energy Mode-Locked Ytterbium-Doped Fiber Laser with Bismuth Telluride Nanosheet Saturable Absorber. *Crystals* **2022**, *12*, 1507. <https://doi.org/10.3390/cryst12111507>

Academic Editor: Ikai Lo

Received: 29 September 2022

Accepted: 21 October 2022

Published: 24 October 2022

**Publisher's Note:** MDPI stays neutral with regard to jurisdictional claims in published maps and institutional affiliations.



**Copyright:** © 2022 by the authors. Licensee MDPI, Basel, Switzerland. This article is an open access article distributed under the terms and conditions of the Creative Commons Attribution (CC BY) license (<https://creativecommons.org/licenses/by/4.0/>).

**Keywords:** YDFL; saturable absorber; mode-locked; fiber laser; bismuth telluride

## 1. Introduction

Pulse fiber lasers are commonly used in a broad spectrum of applications from material processing to medicine and spectroscopy [1–3]. Important criteria of a pulse fiber laser for critical applications that require cleaner finishing from laser cutting are the pulse width and repetition rate. High-power fiber lasers are highly sought after to be used in welding to weld thick metal plates, and in LIDAR technology to obtain high-resolution and high-refresh-rate operation [4]. In view of this, researchers are working around pulse fiber lasers using rare earth ytterbium, which can offer a broad-gain spectrum, high output power, and excellent power conversion efficiency [5].

Various techniques were adopted to generate a pulse in a fiber laser. These encompass artificial (nonlinear polarization rotation [6] and nonlinear amplifying loop mirror [7]) and real saturable absorbers (SA) [8]. Among all these techniques, SA technology is a popular method that relies on material saturable absorption capability to initiate pulsing. Semiconductor SA is well established commercially because of the advances and innovations in engineering technology that allow precise control of its absorption wavelength and saturable fluence [9]. Even though semiconductor SA is already mature, researchers are still working to search for other novel materials with faster relaxation time beyond picoseconds with lower costs to replace semiconductors. This eventually led to the discovery of 2D graphene [10,11] and later to the emergence of graphene oxide (GO) [12,13] carbon nanotube (CNT) [14,15] transition-metal dichalcogenide (TMD) [16,17], topological insulator (TI) [18,19], photonic Floquet topological insulator (PFTI) [20], black phosphorous (BP) [13,21], and MXene [22,23]. These materials offer distinct yet complementary electrical and optical properties. This paves the way for a new opportunity to explore the application of 2D SA in a fiber laser, specifically with ytterbium fiber, to produce high-power lasers.

Recently, the rise of the 2D topological insulator (TI) SA has been gaining attention among researchers. Interestingly, TI is a new kind of quantum electronics matter that exhibits metallic states at the surface but insulates at its interior [24]. TI possesses extraordinary charge and spin properties on the edge and is actively investigated in quantum and spintronic devices [25]. The surface of TI exhibits time-reversal symmetry, which can prevent scattering by other nonmagnetic impurities. TI is validated to demonstrate broadband saturable absorption, large modulation depth, and strong saturable intensity [26]. Additionally, TI also possesses excellent thermoelectric efficiency of 1.34 over 400 K for 24 h with annealed Bi<sub>2</sub>Te<sub>2</sub>/Bi<sub>2</sub>Te<sub>3</sub> core/shell nanosheets [27]. Bernard et al. [28] first investigated the transmission spectrum of Bi<sub>2</sub>Te<sub>3</sub> and confirmed the nonlinear transmission and its saturable absorber behavior at telecommunication wavelength. In the same year, Zhao et al. [29] demonstrated a soliton pulse using an erbium gain medium with a pulse width of 1.21 ps and a repetition rate of 1.21 MHz. They also described the modulation depth of the fabricated TI SA as being as high as 95% and suggested that the high modulation depth of TI is suitable for high-power pulse formation. Successively, TI such as Bi<sub>2</sub>Se<sub>3</sub>, Bi<sub>2</sub>Te<sub>3</sub>, and Sb<sub>2</sub>Te<sub>3</sub> were proven as efficient SA for Q-switching [30–34] and mode-locking [35–42]. Another interesting work that reported using ytterbium-doped fiber was about depositing Sb<sub>2</sub>Te<sub>3</sub> on a side-polished fiber, and producing a pulse width of 5.9 ps and a repetition rate of 19.28 MHz [43,44]. Yan et al. [18] successfully deposited Bi<sub>2</sub>Te<sub>3</sub> in a photonic crystal fiber (PCF) and inserted it into a ring cavity with ytterbium as gain medium. It resulted in a pulse width of 960 ps and a repetition rate of 1.11 MHz. Bi<sub>2</sub>Te<sub>3</sub> was reported to have carrier mobility as high as 5000 cm<sup>2</sup>/(Vs) and an energy bandgap similar to graphene at 0.17 eV [45]. Therefore, Bi<sub>2</sub>Te<sub>3</sub> is expected to operate in a wide wavelength range. Here, we report the mode-locked pulse generation from ytterbium-doped fiber laser (YDFL) using Bi<sub>2</sub>Te<sub>3</sub> SA. The pulse oscillated at a frequency of 9.5 MHz with a pulse width of 600 ps. Efforts were put into manipulating the factors that affect the mode-locking operation, including laser diode pump power, the modulation depth of SA, dispersion, nonlinearity, and gain and loss of a cavity. Adjustment on these parameters resulted in a low pulsing threshold at 85 mW, delivering pulse energy as high as 2.13 nJ. Moreover, it can be concluded from Raman spectroscopy that a thin Bi<sub>2</sub>Te<sub>3</sub> nanosheet was successfully fabricated, and it demonstrated nonlinear saturable absorption in the 1 μm region.

## 2. Preparation and Characterization of Topological Insulator-Based Bi<sub>2</sub>Te<sub>3</sub> Nanosheet SA

This section describes the preparation of Bi<sub>2</sub>Te<sub>3</sub> SA. By using a magnetic hotplate stirrer, 5 mg of Bi<sub>2</sub>Te<sub>3</sub> nanosheets were dispersed in 50 mL of isopropyl alcohol. Once it was evenly dispersed, it was put under an ultra-sonication bath (Branson 2510, 40 kHz) for 2 h at room temperature to produce a homogeneous Bi<sub>2</sub>Te<sub>3</sub> nanosheet solution. Figure 1a shows the produced Bi<sub>2</sub>Te<sub>3</sub> nanosheet solution. After this process, Bi<sub>2</sub>Te<sub>3</sub> suspension was produced with a slightly grey color, which indicates the Bi<sub>2</sub>Te<sub>3</sub> was evenly distributed, as referred to in Figure 1b. Next, the optical deposition technique was adopted with the purpose of attaching Bi<sub>2</sub>Te<sub>3</sub> nanosheets at the end of the fiber ferrule [42,46]. The optical deposition technique was graphically illustrated in Figure 1c. The tip of the fiber ferrule was soaked in a Bi<sub>2</sub>Te<sub>3</sub> suspension solution. At the same time, light from a 980 nm laser diode with pump power fixed at 50 mW was introduced to the fiber ferrule. This process lasted for about 20 min, and the fiber ferrule was removed from the solution to allow evaporation. The fiber ferrule was left to dry for about 15 min. This process was repeated for three rounds to ensure the Bi<sub>2</sub>Te<sub>3</sub> has attached adequately to the fiber ferrule. The ready Bi<sub>2</sub>Te<sub>3</sub> was characterized first before being inserted into the laser cavity.

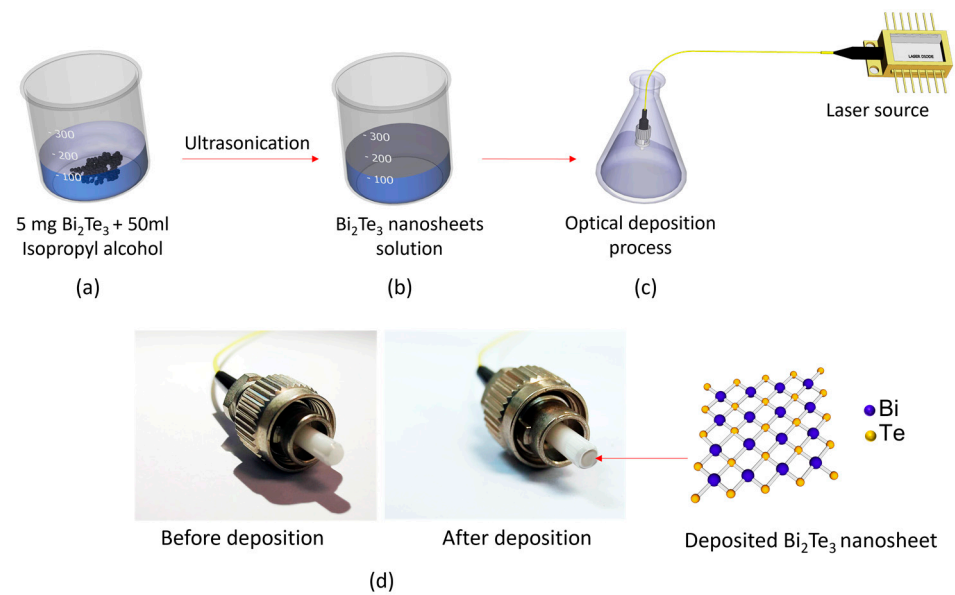


**Figure 1.** Preparation of Bi<sub>2</sub>Te<sub>3</sub> SA: (a) Bi<sub>2</sub>Te<sub>3</sub> nanosheets solution before ultrasonic bath; (b) Bi<sub>2</sub>Te<sub>3</sub> nanosheets solution after ultrasonic bath treatment; (c) optical deposition technique to append Bi<sub>2</sub>Te<sub>3</sub> at the of fiber ferrule; and (d) actual image of before and after Bi<sub>2</sub>Te<sub>3</sub> deposition on fiber ferrule tip.

The properties of successfully prepared Bi<sub>2</sub>Te<sub>3</sub> were further characterized using field-emission scanning electron microscopy (FESEM), Raman spectroscopy, and EDX analysis. Before characterization, the mixture was first dispensed at 600 rpm to wet the copper plate base. The spin speed was increased to 2000 rpm for 45 s to allow Bi<sub>2</sub>Te<sub>3</sub> suspension to spread. Next, the dispensed Bi<sub>2</sub>Te<sub>3</sub> was dried in an oven (80 °C temperature for 60 s) to remove any residual liquid and ready it for morphological characterization. The FESEM image of Bi<sub>2</sub>Te<sub>3</sub> is shown in Figure 2a. The image reveals layers like complex flakes. According to the atomic force microscopy (AFM) topography measurement in Figure 2b, Bi<sub>2</sub>Te<sub>3</sub> was found to have a thickness of about 20 nm. On the other hand, qualitative chemical analysis was performed using EDX, as presented in Figure 2c. It shows that it consists of 52.76 weight % Bi and 47.24 weight % Te elements. Figure 2d illustrates the Raman spectrum at 39.6, 59.5, 100.9, 115, and 136 cm<sup>-1</sup>, respectively. These four Raman optical phonon peaks corresponded to the E<sub>g</sub><sup>1</sup>, A<sub>1g</sub><sup>1</sup>, E<sub>g</sub><sup>2</sup>, A<sub>1u</sub><sup>2</sup>, and A<sub>1g</sub><sup>2</sup> signals. The observed signal peaks are very near to a few-quintuple layer (FQL), 10 quintuple (QL), and 50 QL 2D nanoplate of Bi<sub>2</sub>Te<sub>3</sub> Raman peaks that have previously been reported [47,48]. The Raman analysis was qualitatively similar to that work. An additional peak at 115 cm<sup>-1</sup> was observed as well. This highest peak represents the A<sub>1u</sub> mode composed of longitudinal optical (LO) phonons at the BZ boundary (Z point). This peak was detected as the result of symmetry breaking, proving that the fabricated Bi<sub>2</sub>Te<sub>3</sub> was in a good nano-structured state. The incomplete QL layer at the surface caused atoms at the surface to move out of the plane and this resulted in the presence of an A<sub>1u</sub> mode. Light from a white light source was injected into Bi<sub>2</sub>Te<sub>3</sub>, and its transmission spectrum was recorded via an optical spectrometer. Its linear transmission curve is shown in Figure 2e, covering a broad wavelength with flat linear absorption. This indicates that Bi<sub>2</sub>Te<sub>3</sub> has a broadband optical response. Its nonlinear optical responses, such as saturation intensity, modulation depth, and non-saturable absorption, were also investigated. Details on the nonlinear optical response measurement can be found in [49]. The nonlinear transmission curve is shown in Figure 2f. It was plotted with the equation  $T(I) = 1 - (\alpha_s / (1 + I/I_{sat}) + \alpha_{ns})$ , where  $T(I)$  is the transmission,  $\alpha_s$  is the modulation depth,  $I$  is the input intensity,  $I_{sat}$  is the saturation intensity, and  $\alpha_{ns}$  is the nonsaturable absorption. From the fitted graph, it can be determined that the saturation intensity  $I_{sat}$  for Bi<sub>2</sub>Te<sub>3</sub> is 10.2 MW/cm<sup>2</sup>, modulation depth is at 41.4%, and nonsaturable absorption is measured at 10%. The  $I_{sat}$  of 10.2 MW/cm<sup>2</sup> is taken when the power intensity reduces the absorption to half of its unbleached value. The modulation depth refers to the maximum change in

transmission (distance between two dotted blue lines), while nonsaturable absorption is measured from the saturation curve at 90% to the maximum. The error bar analysis reveals minimum and maximum errors of 0.07% and 3.89%, respectively.

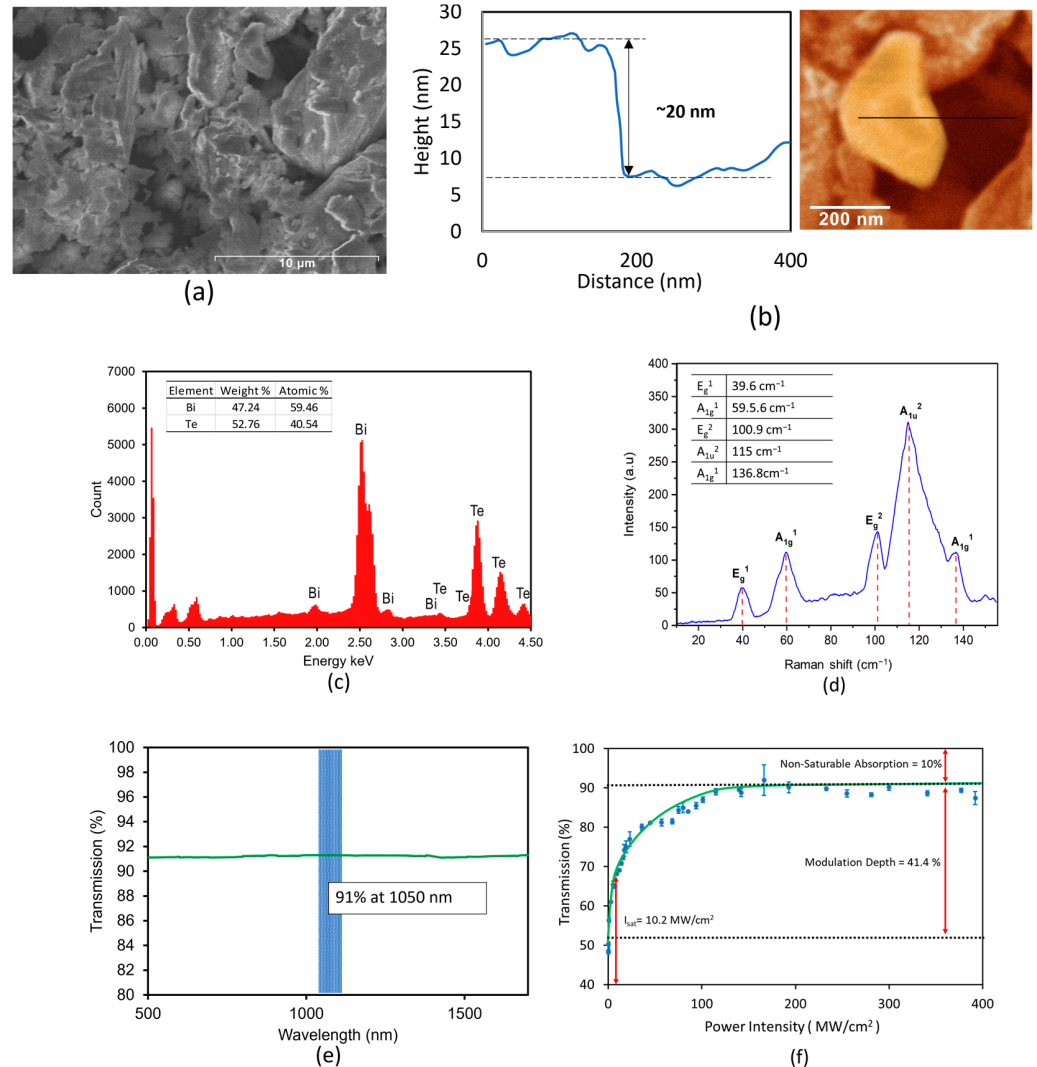


**Figure 2.** Characterization of  $\text{Bi}_2\text{Te}_3$ : (a) FESEM image; (b) AFM topography of  $\text{Bi}_2\text{Te}_3$ ; (c) EDX analysis; (d) Raman spectrum; (e) linear transmission spectrum; and (f) nonlinear transmission curve.

### 3. Experimental Setup

Figure 3 shows the proposed experimental setup. It uses 1 m long ytterbium-doped fiber (YDF) as a gain medium. The characteristics of YDF are as follows: core and cladding diameters of 4  $\mu\text{m}$  and 125  $\mu\text{m}$ , respectively, numerical aperture (NA) of 0.20, a cut-off wavelength at 1010 nm, ytterbium ion absorption of 280 dB/m at 920 nm, and group velocity dispersion (GVD) of 24.22  $\text{ps}^2/\text{km}$ . A 980/1064 nm wavelength division multiplexer (WDM) multiplexed 980 nm laser diode (LD) and lasing from YDF. The prepared  $\text{Bi}_2\text{Te}_3$  SA was carefully arranged inside the laser cavity to induce pulsing. SA insertion loss was estimated at around 4 dB at the 1050 nm wavelength. The role of an isolator is to force one direction of light operation. A 50/50 coupler was used to tap out a portion of light for monitoring while retaining the remaining 50% for further oscillation. The monitoring instruments involved were an optical spectrum analyzer (OSA, Yokogawa AQ6370B), an oscilloscope (LeCroy, 352A), and a 7.8 GHz radio-frequency (RF, Anritsu MS2683A) spectrum analyzer. A 1.2 GHz InGaAs photodetector (Thorlabs DET01CFC) was employed to convert the optical into an electrical signal for further analysis. The length of

the laser cavity was projected at 18 m. Except for the gain medium, the cavity was made up of single-mode fiber (HI 1060) with GVD  $-21. \text{ps}^2/\text{km}$ . The laser cavity's dispersion was estimated at  $-19.9 \text{ps}^2/\text{km}$ .

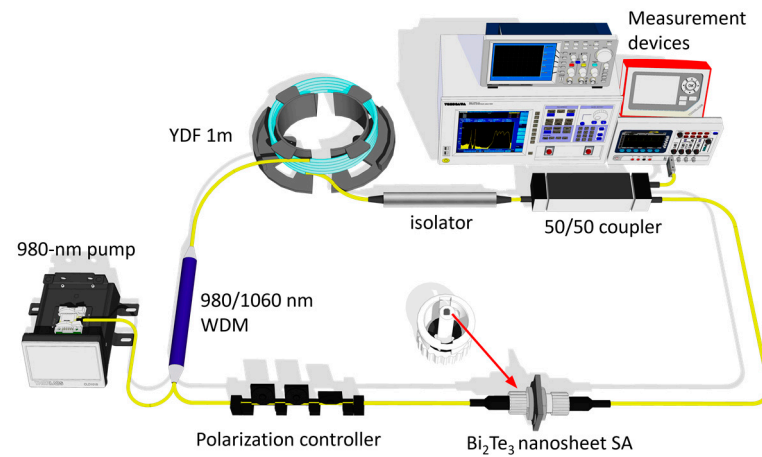


**Figure 3.** Proposed configuration of the mode-locked YDFL with  $\text{Bi}_2\text{Te}_3$  SA.

#### 4. Results and Discussion

The laser diode pump power was slowly increased, and once pump power reached around 85 mW, the continuous-wave (CW) lasing was observed to change to pulsing operation. Pump power was further increased up to 203.5 mW, and pulsing was still observed and maintained. The pulsing spectrum at the pump power of 203.5 mW was recorded with an optical spectrum analyzer (OSA). Figure 4 illustrates the optical spectrum, spanning from 1035 nm to 1060 nm. The center of the spectrum was located at 1050.23 nm, with a 3 dB bandwidth of 2.3 nm. No clear Kelly sidebands were visible on the optical spectrum, suggesting that the pulse was chirped because of the long-constructed cavity.

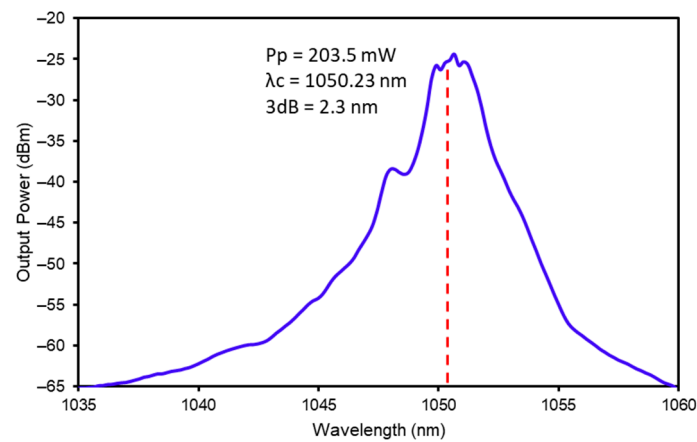


**Figure 4.** Optical spectrum of the mode-locked YDFL at pump power of 203.5 mW, centered at 1050.23 nm.

Figure 5a reveals the temporal characteristics of the generated pulse at the pump power of 203.5 mW. The peak-to-peak of the oscillation pulse in Figure 5b was consistently separated at 105.26 ns, equivalent to a repetition rate of 9.5 MHz. This fundamental frequency matched the cavity length. The pulse width was measured to be 600 ps at the oscilloscope. The pulse width was predicted to be less than 0.5 ps if the trace is fitted to a sech pulse profile with a time-bandwidth profile (TBP) = 0.315.



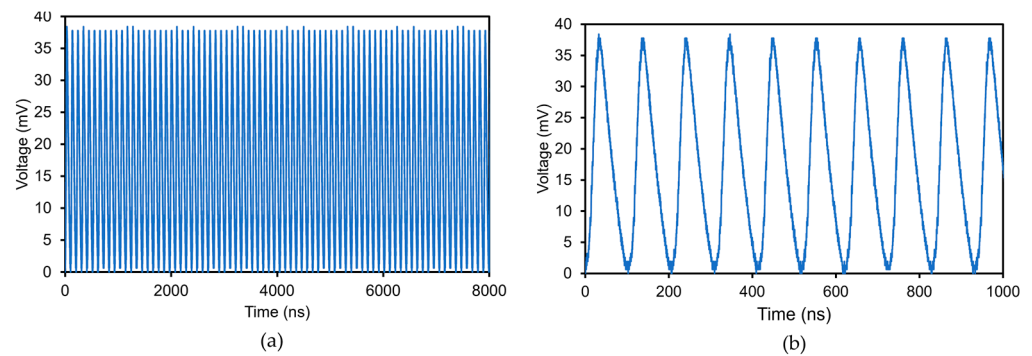


**Figure 5.** Typical temporal characteristics of the mode-locked YDFL: (a) zoom-out oscillation trace at the pump power of 203.5 mW and (b) zoom-in oscillation trace showing the separation between oscillation trace.

Nevertheless, the actual pulse width was larger because of the long cavity, which introduced chirping. Figure 6 projects the radio-frequency spectrum of the mode-locked pulse. A solid signal peak at a fundamental repetition rate of 9.5 MHz was clearly shown at the spectrum analyzer. The signal-to-noise ratio (SNR) measurement was examined at 44 dB. This proved that the mode-locking emission was steady and stable in the laboratory environment.

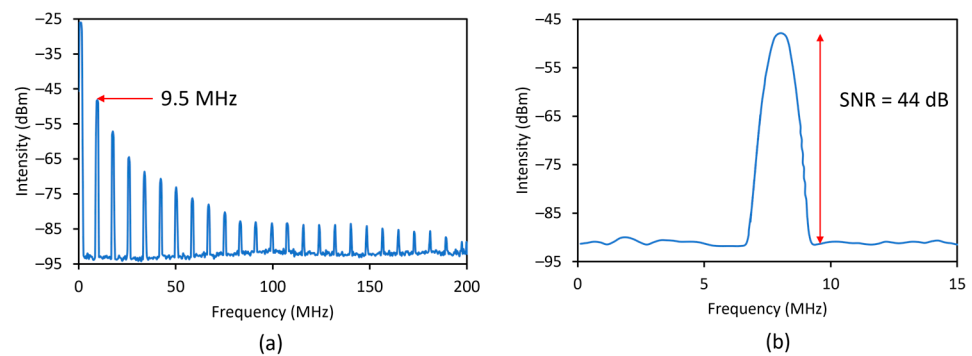


**Figure 6.** RF spectrum of the mode-locked YDFL: (a) radio frequency showing the harmonics of a pulse and (b) SNR measurement of 44 dB at a fundamental frequency.

Figure 7 shows the measured output power of the mode-locked YDFL with laser diode pump power ranging from 85 mW to 203.5 mW. A power meter was used to measure the average output power of mode-locked YDFL. The pulse energy was calculated and projected in Figure 7. Both pulse output power and pulse energy increased with pump power from threshold mode-locking power to 203.5 mW. The highest attainable output power and pulse energy were 20.3 mW and 2.13 nJ, respectively. The pulse peak power was anticipated to be 3.76 kW. The laser slope efficiency was calculated from the output power data at 10.2%. When the laser diode pump power was further raised beyond 20.3 mW, pulsing became unstable and fluctuated. The unstable pulsing was due to the over-saturation of SA. The pump power was reduced slowly to below 203.5 mW, and the pulsing appeared stable. It can be concluded that the thermal power from the laser diode did not accumulate at SA and destroy it. On another note, no pulsing was initiated when the SA was removed from the cavity. The PC was rotated in a wide orientation, yet no pulsing was discovered. This proved that the fabricated SA is the key element, and the pulsing was contributed to by the saturable absorption characteristics of the SA. Figure 8 illustrates the wavelength stability. The stability of center wavelength of optical spectrum was checked in three hours. The center wavelength was centered around 1050 nm and the recorded maximum fluctuation was recorded at 0.006%. The output power was consistently measured at around 20.3 mW, with a fluctuation of 0.34%.

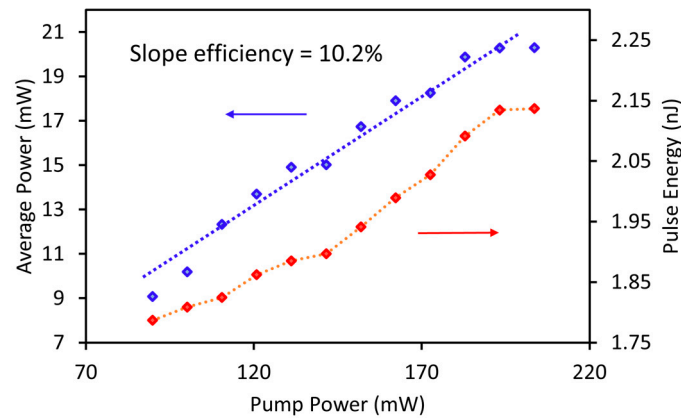


**Figure 7.** Correlation between average output power and pulse with 980 nm pump power for the mode-locked YDFL.

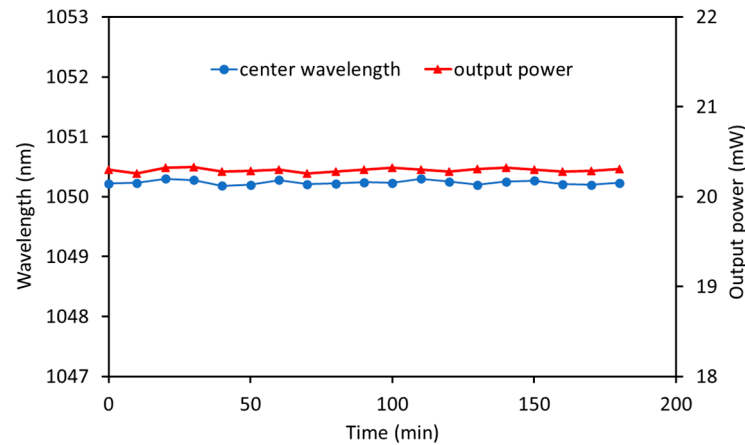


**Figure 8.** Stability test of mode-locked YDFL optical spectrum and output power.

Table 1 below summarizes the published work on mode-locked YDFL with  $\text{Bi}_2\text{Te}_3$  SA. Various integration techniques of  $\text{Bi}_2\text{Te}_3$  were adopted, such as depositing  $\text{Bi}_2\text{Te}_3$  at the end of the fiber ferrule, side-polished fiber (SPF), tapered fiber, and filling up the photonic crystal fiber (PCF). The mode-locking threshold in our work was relatively low at 85 mW, and the pulse energy is high at 2 nJ.

**Table 1.** Mode-locked YDFL based on  $\text{Bi}_2\text{Te}_3$  SA.

| Integration Method | Center Wavelength | 3 dB Bandwidth | Threshold (mW) | Pulse Energy | Pulse Width | Repetition Rate | Ref       |
|--------------------|-------------------|----------------|----------------|--------------|-------------|-----------------|-----------|
| SPF                | 1057.82 nm        | 3.69 nm        | 200 mW         | 0.599 nJ     | 230 ps      | 1.44 MHz        | [50]      |
| Tapered fiber      | 1052.5 nm         | 1.245 nm       | 230 mW         | 2.8 nJ       | 317 ps      | 19.8 MHz        | [51]      |
| PCF                | 1064.47 nm        | 1.11 nm        | 115 mW         | 1 nJ         | 960 ps      | 1.11 MHz        | [18]      |
| Fiber ferrule      | 1052.7 nm         | 0.45 nm        | 75 mW          | 753.9 pJ     | 417 ps      | 25.6 MHz        | [52]      |
| Tapered fiber      | 1063.4 nm         | 2.24 nm        | 220 mW         | 2 nJ         | 5.47 ns     | 6.2 MHz         | [53]      |
| Fiber ferrule      | 1050.23 nm        | 2.3 nm         | 85 mW          | 2.13 nJ      | 600 ps      | 9.5 MHz         | This Work |

## 5. Conclusions

Mode-locked YDFL with  $\text{Bi}_2\text{Te}_3$  SA was successfully demonstrated. The fabricated SA was in a good nano-structured state and exhibited modulation depth of 41.4%, favoring mode-locking operation. The generated pulse was stable in the laboratory with a repetition rate of 9.5 MHz. The fluctuation of the repetition rate is small, with a maximum fluctuation of 0.53%. The pulse energy recorded from this mode-locked YDFL was high at 2.13 nJ. This proves that the in-house fabricated  $\text{Bi}_2\text{Te}_3$  SA is a promising broadband SA element suitable for various medical and industrial processing applications.

**Author Contributions:** Conceptualization, methodology and validation, H.H., A.R.M. and T.S.J.; resources, I.S.; formal analysis, M.M.I.M.H.; writing—original draft preparation, H.H.; writing—review and editing, H.H., A.R.M., T.S.J. and A.M.M.; visualization, A.R.M. and M.H.I.; supervision, I.S.; project administration and funding acquisition, I.S. and M.B. All authors have read and agreed to the published version of the manuscript.

**Funding:** This research was funded by the Niche Research Fund Scheme, Universiti Malaysia Sabah (UMS), grant number SDN00286, and the Postgraduate Research Grant Scheme (UMSGreat), grant number GUG0444-1/2020, and UOW Malaysia KDU Malaysia, grant number (KDURG/2019/1/004). The APC was funded by I. Saad.

**Data Availability Statement:** Not applicable.

**Acknowledgments:** The authors would also like to thank the research facilities at the Photonics Engineering Laboratory, University of Malaya (UM), the Nanophotonics Laboratory, Institute of Microengineering and Nanoelectronics, Universiti Kebangsaan Malaysia (UKM), and INTI International University for the research support. This project is also funded by the Ministry of Higher Education Malaysia under the Fundamental Research Grant Scheme (FRGS), with a reference number of FRGS/1/2022/TK08/UMS/02/17.

**Conflicts of Interest:** The authors declare no conflict of interest.

## References

1. Bliedtner, J.; Schindler, C.; Seiler, M.; Wächter, S.; Friedrich, M.; Giesecke, J. Ultrashort pulse laser material processing: An extension of application variety for ultrashort pulse laser processing of different materials. *Laser Tech. J.* **2016**, *13*, 46–50. [[CrossRef](#)]
2. Plamann, K.; Aptel, F.; Arnold, C.; Courjaud, A.; Crotti, C.; Deloison, F.; Druon, F.; Georges, P.; Hanna, M.; Legeais, J.-M. Ultrashort pulse laser surgery of the cornea and the sclera. *J. Opt.* **2010**, *12*, 084002. [[CrossRef](#)]
3. Nicolodelli, G.; Senesi, G.S.; Romano, R.A.; de Perazzoli, I.L.O.; Milori, D.M.B.P. Signal enhancement in collinear double-pulse laser-induced breakdown spectroscopy applied to different soils. *Spectrochim. Acta B Atomic Spectrosc.* **2015**, *111*, 23–29. [[CrossRef](#)]
4. Kim, G.; Park, Y. LIDAR pulse coding for high resolution range imaging at improved refresh rate. *Opt. Express* **2016**, *24*, 23810–23828. [[CrossRef](#)]
5. Pan, L.; Utkin, I.; Fedosejevs, R. Two-wavelength passively Q-switched ytterbium doped fiber laser. *Opt Express* **2008**, *16*, 11858–11870. [[CrossRef](#)]
6. Tan, S.J.; Tiu, Z.C.; Harun, S.W.; Ahmad, H. Sideband-controllable soliton pulse with bismuth-based erbium-doped fiber. *Chin. Opt. Lett.* **2015**, *13*, 111406. [[CrossRef](#)]
7. Michalska, M.; Swiderski, J. Noise-like pulse generation using polarization maintaining mode-locked thulium-doped fiber laser with nonlinear amplifying loop mirror. *IEEE Photonics J.* **2019**, *11*, 1–10. [[CrossRef](#)]
8. Kisel, V.; Rudenkov, A.; Pavlyuk, A.; Kovalyov, A.; Preobrazhenskii, V.; Putyato, M.; Rubtsova, N.; Semyagin, B.; Kuleshov, N. High-power, efficient, semiconductor saturable absorber mode-locked Yb: KGW bulk laser. *Opt. Lett.* **2015**, *40*, 2707–2710. [[CrossRef](#)]
9. Pogaku, D.; Saad, I. Effects of S/D doping concentrations on strained SiGe vertical I-MOS characteristics. In Proceedings of the 2011 3rd International Conference on Electronics Computer Technology, Kanyakumari, India, 8–10 April 2011; pp. 294–297.
10. Zhang, H.; Tang, D.; Zhao, L.; Bao, Q.; Loh, K. Large energy mode locking of an erbium-doped fiber laser with atomic layer graphene. *Opt. Express* **2009**, *17*, 17630–17635. [[CrossRef](#)]
11. Zhang, Z.; Wang, R.; Zhang, Y.; Kartashov, Y.V.; Li, F.; Zhong, H.; Guan, H.; Gao, K.; Li, F.; Zhang, Y. Observation of edge solitons in photonic graphene. *Nat. Commun.* **2020**, *11*, 1902. [[CrossRef](#)]
12. Adnan, N.; Bidin, N.; Taib, N.; Haris, H.; Fakaruddin, M.; Hashim, A.; Krishnan, G.; Harun, S.W. Passively Q-switched flashlamp pumped Nd: YAG laser using liquid graphene oxide as saturable absorber. *Opt. Laser Technol.* **2016**, *80*, 28–32. [[CrossRef](#)]
13. Markom, A.; Tan, S.; Muhammad, A.; Paul, M.C.; Dhar, A.; Das, S.; Latiff, A.; Harun, S. Dark pulse mode-locked fibre laser with zirconia-based erbium-doped fibre (Zr-EDF) and Black phosphorus saturable absorber. *Optik* **2020**, *223*, 165635. [[CrossRef](#)]
14. Taib, N.A.M.; Bidin, N.; Haris, H.; Adnan, N.N.; Ahmad, M.F.S.; Harun, S.W. Multi-walled carbon nanotubes saturable absorber in Q-switching flashlamp pumped Nd: YAG laser. *Chin. Phys. Lett.* **2016**, *79*, 193–197.
15. Ahmad, F.; Haris, H.; Nor, R.; Zulkepely, N.; Ahmad, H.; Harun, S. Passively Q-switched EDFL using a multi-walled carbon nanotube polymer composite based on a saturable absorber. *Chin. Phys. Lett.* **2014**, *31*, 034204. [[CrossRef](#)]
16. Kadir, N.; Ismail, E.I.; Latiff, A.A.; Ahmad, H.; Arof, H.; Harun, S.W. Transition metal dichalcogenides (WS<sub>2</sub> and MoS<sub>2</sub>) saturable absorbers for mode-locked erbium-doped fiber lasers. *Chin. Phys. Lett.* **2017**, *34*, 014202. [[CrossRef](#)]
17. Chen, H.; Yin, J.; Yang, J.; Zhang, X.; Liu, M.; Jiang, Z.; Wang, J.; Sun, Z.; Guo, T.; Liu, W. Transition-metal dichalcogenides heterostructure saturable absorbers for ultrafast photonics. *Opt. Lett.* **2017**, *42*, 4279–4282. [[CrossRef](#)]
18. Yan, P.; Lin, R.; Chen, H.; Zhang, H.; Liu, A.; Yang, H.; Ruan, S. Topological insulator solution filled in photonic crystal fiber for passive mode-locked fiber laser. *IEEE Photonics Technol. Lett.* **2014**, *27*, 264–267.



19. Luo, Z.; Liu, C.; Huang, Y.; Wu, D.; Wu, J.; Xu, H.; Cai, Z.; Lin, Z.; Sun, L.; Weng, J. Topological-insulator passively Q-switched double-clad Fiber laser at 2 $\mu$ m wavelength. *IEEE J. Sel. Top. Quantum Electron.* **2014**, *20*, 1–8.
20. Zhang, Y.; Wu, Z.; Belić, M.R.; Zheng, H.; Wang, Z.; Xiao, M.; Zhang, Y. Photonic Floquet topological insulators in atomic ensembles. *Laser Photonics Rev.* **2015**, *9*, 331–338. [[CrossRef](#)]
21. Li, J.; Luo, H.; Zhai, B.; Lu, R.; Guo, Z.; Zhang, H.; Liu, Y. Black phosphorus: A two-dimension saturable absorption material for mid-infrared Q-switched and mode-locked fiber lasers. *Sci. Rep.* **2016**, *6*, 30361. [[CrossRef](#)]
22. Wu, Q.; Jin, X.; Chen, S.; Jiang, X.; Hu, Y.; Jiang, Q.; Wu, L.; Li, J.; Zheng, Z.; Zhang, M. MXene-based saturable absorber for femtosecond mode-locked fiber lasers. *Opt. Express* **2019**, *27*, 10159–10170. [[CrossRef](#)] [[PubMed](#)]
23. Li, J.; Zhang, Z.; Du, L.; Miao, L.; Yi, J.; Huang, B.; Zou, Y.; Zhao, C.; Wen, S. Highly stable femtosecond pulse generation from a MXene Ti<sub>3</sub>C<sub>2</sub>T<sub>x</sub> (T = F, O, or OH) mode-locked fiber laser. *Photonics Res.* **2019**, *7*, 260–264. [[CrossRef](#)]
24. Tian, W.; Yu, W.; Shi, J.; Wang, Y. The property, preparation and application of topological insulators: A review. *Materials* **2017**, *10*, 814. [[CrossRef](#)] [[PubMed](#)]
25. Yue, Z.; Wang, X.; Gu, M. Topological insulator materials for advanced optoelectronic devices. In *Advanced Topological Insulators*; John and Wiley and Sons: Hoboken, NJ, USA; Scrivener Publishing LLC.: Beverly, MA, USA, 2019; pp. 45–70.
26. Peiguang, Y.; Rongyong, L.; Han, Z.; Zhiteng, W.; Han, C.; Shuangchen, R. Multi-pulses dynamic patterns in a topological insulator mode-locked ytterbium-doped fiber laser. *Opt. Commun.* **2015**, *335*, 65–72. [[CrossRef](#)]
27. Bauer, C.; Veremchuk, I.; Kunze, C.; Benad, A.; Dzhagan, V.M.; Haubold, D.; Pohl, D.; Schiering, G.; Nielsch, K.; Lesnyak, V. Heterostructured bismuth telluride selenide nanosheets for enhanced thermoelectric performance. *Small Sci.* **2021**, *1*, 2000021. [[CrossRef](#)]
28. Bernard, F.; Zhang, H.; Gorza, S.-P.; Emplit, P. Towards mode-locked fiber laser using topological insulators. In Proceedings of the Nonlinear Photonics, Colorado Springs, CO, USA, 17–21 June 2012; p. NTh1A. 5.
29. Zhao, C.; Zhang, H.; Qi, X.; Chen, Y.; Wang, Z.; Wen, S.; Tang, D. Ultra-short pulse generation by a topological insulator based saturable absorber. *Appl. Phys. Lett.* **2012**, *101*, 211106. [[CrossRef](#)]
30. Yu, Z.H.; Song, Y.R.; Tian, J.R.; Dou, Z.Y.; Guoyu, H.Y.; Li, K.X.; Li, H.W.; Zhang, X.P. High-repetition-rate Q-switched fiber laser with high quality topological insulator Bi<sub>2</sub>Se<sub>3</sub> film. *Opt. Express* **2014**, *22*, 11508–11515. [[CrossRef](#)]
31. Luo, Z.; Huang, Y.; Weng, J.; Cheng, H.; Lin, Z.; Xu, B.; Cai, Z.; Xu, H. 1.06  $\mu$ m Q-switched ytterbium-doped fiber laser using few-layer topological insulator Bi<sub>2</sub>Se<sub>3</sub> as a saturable absorber. *Opt. Express* **2013**, *21*, 29516–29522. [[CrossRef](#)]
32. Sun, Y.-J.; Lee, C.-K.; Wang, Y.; Xia, H.-P.; Wang, X.-H.; You, Z.-Y.; Tu, C.-Y.; Xu, J.-L. Passively Q-Switched Wavelength-Tunable Bulk Laser Using Topological Insulator at 1  $\mu$ m. *IEEE Photonics Technol. Lett.* **2016**, *28*, 2764–2767. [[CrossRef](#)]
33. Wu, M.; Chen, Y.; Zhang, H.; Wen, S.J.I.J.o.Q.E. Nanosecond Q-Switched Erbium-Doped Fiber Laser With Wide Pulse-Repetition-Rate Range Based on Topological Insulator. *IEEE J. Quantum Electron* **2014**, *50*, 393–396.
34. Lee, J.; Lee, J.; Koo, J.; Chung, H.; Lee, J.H. Linearly polarized, Q-switched, erbium-doped fiber laser incorporating a bulk-structured bismuth telluride/polyvinyl alcohol saturable absorber. *Opt. Eng.* **2016**, *55*, 076109. [[CrossRef](#)]
35. Lee, J.; Koo, J.; Jhon, Y.M.; Lee, J.H. A femtosecond pulse erbium fiber laser incorporating a saturable absorber based on bulk-structured Bi<sub>2</sub>Te<sub>3</sub> topological insulator. *Opt. Express* **2014**, *22*, 6165–6173. [[CrossRef](#)] [[PubMed](#)]
36. Dou, Z.Y.; Song, Y.R.; Tian, J.R.; Liu, J.H.; Yu, Z.H.; Fang, X.H. Mode-locked ytterbium-doped fiber laser based on topological insulator: Bi<sub>2</sub>Se<sub>3</sub>. *Opt. Express* **2014**, *22*, 24055–24061. [[CrossRef](#)] [[PubMed](#)]
37. Yin, K.; Zhang, B.; Li, L.; Jiang, T.; Zhou, X.; Hou, J. Soliton mode-locked fiber laser based on topological insulator Bi<sub>2</sub>Te<sub>3</sub> nanosheets at 2  $\mu$ m. *Photonics Res.* **2015**, *3*, 72. [[CrossRef](#)]
38. Duan, L.; Wang, Y.; Xu, C.; Li, L.; Wang, Y. Passively Harmonic Mode-Locked Fiber Laser With a High Signal-to-Noise Ratio via Evanescent-Light Deposition of Bismuth Telluride (Bi<sub>2</sub>Te<sub>3</sub>) Topological Insulator Based Saturable Absorber. *IEEE Photonics J.* **2015**, *7*, 1–7. [[CrossRef](#)]
39. Wei, Q.; Niu, K.; Han, X.; Zhang, H.; Zhang, C.; Yang, C.; Man, B. Large energy pulses generation in a mode-locked Er-doped fiber laser based on CVD-grown Bi<sub>2</sub>Te<sub>3</sub> saturable absorber. *Opt. Mater. Express* **2019**, *9*, 3535–3545. [[CrossRef](#)]
40. Wei, Q.; Han, X.; Zhang, H.; Yang, C.; Zhang, C.; Gao, J.; Man, B.; Xu, S. CVD-Bi<sub>2</sub>Te<sub>3</sub> as a saturable absorber for various solitons in a mode-locked Er-doped fiber laser. *Appl. Opt.* **2020**, *59*, 7792–7800. [[CrossRef](#)]
41. Lee, J.; Koo, J.; Lee, J.H. A pulse-width-tunable, mode-locked fiber laser based on dissipative soliton resonance using a bulk-structured Bi<sub>2</sub>Te<sub>3</sub> topological insulator. *Opt. Eng.* **2016**, *55*, 081309. [[CrossRef](#)]
42. Haris, H.; Batumalay, M.; Tan, S.J.; Markom, A.M.; Muhammad, A.R.; Harun, S.W.; Hasnan, M.M.I.M.; Saad, I. Mode-Locked YDFL Using Topological Insulator Bismuth Selenide Nanosheets as the Saturable Absorber. *Crystals* **2022**, *12*, 489. [[CrossRef](#)]
43. Kowalczyk, M.; Bogusławski, J.; Zybala, R.; Mars, K.; Mikuła, A.; Soboń, G.; Sotor, J. Sb<sub>2</sub>Te<sub>3</sub>-deposited D-shaped fiber as a saturable absorber for mode-locked Yb-doped fiber lasers. *Opt. Mater. Express* **2016**, *6*, 2273–2282. [[CrossRef](#)]
44. Gao, L.; Zhu, T.; Huang, W.; Luo, Z. Stable, Ultrafast Pulse Mode-Locked by Topological Insulator Bi<sub>2</sub>Se<sub>3</sub> With Photonic Crystal Fiber: From Anomalous Dispersion to Normal Dispersion. *IEEE Photonics J.* **2015**, *7*, 1–8.
45. Lin, Y.-H.; Lin, S.-F.; Chi, Y.-C.; Wu, C.-L.; Cheng, C.-H.; Tseng, W.-H.; He, J.-H.; Wu, C.-I.; Lee, C.-K.; Lin, G.-R. Using n-and p-type Bi<sub>2</sub>Te<sub>3</sub> topological insulator nanoparticles to enable controlled femtosecond mode-locking of fiber lasers. *ACS Photonics* **2015**, *2*, 481–490. [[CrossRef](#)]
46. Woodward, R.I.; Kelleher, E.J. 2D saturable absorbers for fibre lasers. *Appl. Sci.* **2015**, *5*, 1440–1456. [[CrossRef](#)]

47. Russo, V.; Bailini, A.; Zamboni, M.; Passoni, M.; Conti, C.; Casari, C.S.; Bassi, A.L.; Bottani, C.E. Raman spectroscopy of Bi-Te thin films. *J. Raman Spectrosc.* **2008**, *39*, 205–210. [[CrossRef](#)]
48. Shahil, K.; Hossain, M.; Goyal, V.; Balandin, A.A. Micro-Raman spectroscopy of mechanically exfoliated few-quintuple layers of Bi<sub>2</sub>Te<sub>3</sub>, Bi<sub>2</sub>Se<sub>3</sub>, and Sb<sub>2</sub>Te<sub>3</sub> materials. *J. Appl. Phys.* **2012**, *111*, 054305. [[CrossRef](#)]
49. Haris, H.; Harun, S.; Muhammad, A.; Anyi, C.; Tan, S.; Ahmad, F.; Nor, R.; Zulkepely, N.; Arof, H. Passively Q-switched Erbium-doped and Ytterbium-doped fibre lasers with topological insulator bismuth selenide (Bi<sub>2</sub>Se<sub>3</sub>) as saturable absorber. *Opt. Laser Technol.* **2017**, *88*, 121–127. [[CrossRef](#)]
50. Chi, C.; Lee, J.; Koo, J.; Lee, J.H. All-normal-dispersion dissipative-soliton fiber laser at 1.06 μm using a bulk-structured Bi<sub>2</sub>Te<sub>3</sub> topological insulator-deposited side-polished fiber. *Laser Phys.* **2014**, *24*, 105106. [[CrossRef](#)]
51. Li, L.; Yan, P.-G.; Wang, Y.-G.; Duan, L.-N.; Sun, H.; Si, J.-H. Yb-doped passively mode-locked fiber laser with Bi<sub>2</sub>Te<sub>3</sub>-deposited. *Chin. Phys. B* **2015**, *24*, 124204. [[CrossRef](#)]
52. Li, L.; Wang, Y.; Sun, H.; Duan, L.; Wang, X.; Si, J. All-normal dispersion passively mode-locked Yb-doped fiber laser with Bi<sub>2</sub>Te<sub>3</sub> absorber. *Opt. Eng.* **2015**, *54*, 046101. [[CrossRef](#)]
53. Li, L.; Wang, Y.; Wang, X.; Lin, T.; Sun, H. High energy mode-locked Yb-doped fiber laser with Bi<sub>2</sub>Te<sub>3</sub> deposited on tapered-fiber. *Optik* **2017**, *142*, 470–474. [[CrossRef](#)]